



OPEN ACCESS

EDITED BY

Tao Hu,
China University of Petroleum, Beijing, China

REVIEWED BY

Yazhou Liu,
China University of Petroleum, Beijing, China
Tianyu Zheng,
University of Science and Technology,
Beijing, China

*CORRESPONDENCE

Guoyi Hu,
✉ huguoyi69@petrochina.com.cn
Xianqing Li,
✉ Lixq@cumb.edu.cn

RECEIVED 16 February 2025

ACCEPTED 14 March 2025

PUBLISHED 01 April 2025

CITATION

Guo C, Hu G, Li J, Tian X, Tian L, Guo J, Cui H,
Liu Z and Li X (2025) Light hydrocarbons
composition and carbon isotopes unravel the
origin of natural gas in Triassic marine strata of
Moxi gas field, central Sichuan Basin.
Front. Earth Sci. 13:1577658.
doi: 10.3389/feart.2025.1577658

COPYRIGHT

© 2025 Guo, Hu, Li, Tian, Tian, Guo, Cui, Liu
and Li. This is an open-access article
distributed under the terms of the [Creative
Commons Attribution License \(CC BY\)](#). The
use, distribution or reproduction in other
forums is permitted, provided the original
author(s) and the copyright owner(s) are
credited and that the original publication in
this journal is cited, in accordance with
accepted academic practice. No use,
distribution or reproduction is permitted
which does not comply with these terms.

Light hydrocarbons composition and carbon isotopes unravel the origin of natural gas in Triassic marine strata of Moxi gas field, central Sichuan Basin

Chuyuan Guo^{1,2,3}, Guoyi Hu^{2*}, Jin Li², Xingwang Tian⁴,
Lianjie Tian², Jinhao Guo², Huiying Cui², Zhen Liu^{1,2,3} and
Xianqing Li^{1,3*}

¹State Key Laboratory for Fine Exploration and Intelligent Development of Coal Resources, China University of Mining and Technology–Beijing, Beijing, China, ²PetroChina Research Institute of Petroleum Exploration and Development, Beijing, China, ³College of Geoscience and Surveying Engineering, China University of Mining and Technology–Beijing, Beijing, China, ⁴Research Institute of Exploration and Development, PetroChina Southwest Oil & Gas field Company, Chengdu, China

The Triassic marine gas reservoir in the Moxi Gas Field is one of the large gas fields initially discovered in the Sichuan Basin. However, the origin of its natural gas has long been debated. To study the genetic types and origin of natural gas, the light hydrocarbons (LHs) composition, carbon isotopes, chemical compositions, and stable carbon and hydrogen isotopic compositions were analyzed in the Triassic strata of Moxi gas field in the Sichuan Basin. The natural gases from the second member of the Jialingjiang Formation (T_2^j) and the first member of the Leikoupo Formation (T_2^{l1}) have dryness coefficients higher than 0.997 and contain low content non-alkane gases such as CO_2 and N_2 . The $\delta^{13}\text{C}_1$ values of natural gas in the Moxi (MX) gas field range from -35.3% to -32.9% , the $\delta^{13}\text{C}_2$ values range from -34.0% to -30.3% , and the δD_1 values range from -144% to -120% . As for light hydrocarbons composition, the C_7 LHs are dominated by the methylcyclohexane (MCH), and the C_6 – C_7 LHs have low normal alkane contents. The individual carbon isotopes of light hydrocarbons have the characteristics of $\delta^{13}\text{C} > -28\%$. The origin identification indicates that the natural gas in this area is oil-type gas that results from the secondary cracking of crude oil. Our results show that the natural gas in T_2^j of the MX gas field is sourced from the shale gas of the E_1q , the T_2^{l1} gas is a mixed-source gas from different thermal evolution stages of the E_1q source rocks, shale gas and oil-cracking gas. The mixing effect is the main reason for the reversed phenomenon ($\delta^{13}\text{C}_1 > \delta^{13}\text{C}_2$).

KEYWORDS

Moxi gas field, light hydrocarbons, shale gas, genetic types, gas source rock

Highlights

1. The T_2l^1 gas is a mixed-source gas from the shale gas and oil-cracking gas of the E_1q Fm.
2. The mixing effect gives T_2l^1 gas $\delta^{13}C_1 > \delta^{13}C_2$.
3. The dominance of MCH relative to C_7 LHs, $\delta^{13}C_{CH} > -24\text{‰}$ and $\delta^{13}C_{MCP} < \delta^{13}C_{CH}$ distinguish shale gas from oil-cracking gas.

1 Introduction

The MX gas field is located in the southern part of the central Sichuan low-flat tectonic area. The gas-bearing structure is at the top of the eastern segment of the Leshan-Longnyusi Caledonian Paleo-uplift. From bottom to top, there are three pay zones, namely, the gas reservoir in the T_2j^2 and T_2l^1 of the marine strata, and the gas reservoir in the Xujiahe Formation (T_2x) of the continental strata. This gas field spatially overlays the Anyue gas field, a super-large gas field in the Sinian-Cambrian System in central Sichuan. The gas-bearing range of the MX gas field is smaller than that of the Anyue Gas Field. The Leshan-Longnyusi Paleo-uplift developed in the Gaoshiti-Moxi area is the dominant direction for the long-term accumulation of oil and gas migration.

The MX gas field is a large scale gas field discovered relatively early in the Sichuan Basin. The T_2l^1 gas reservoir was proven in 1988, and it took 26 years for the T_2j^2 gas reservoir to be proven (Wang et al., 1998). However, the gas source has been less discussed and exists significant dispute over the source of the gas. Some scholars believe that the gas in T_2l^1 sourced from the coal measures of the Longtan Formation (P_2l) (Wang et al., 1998; Li et al., 2006), and the gas in T_2j^2 is contributed by the Permian carbonate source rocks (Li et al., 2006). However, the burial depth of the Triassic gas reservoir is only more than 2,600 m. The inclusion detection show that the temperature of the fluids trapped in the reservoir is 111–165°C, which has just reached the stage of oil-cracking gas generation, corresponding to the condensate oil and gas generation (Jin et al., 2019). But the gas dryness coefficient is extremely high, with $\delta^{13}C_1$ being heavy while $\delta^{13}C_2$ is light, which is obviously inconsistent with the thermal evolution history of the Permian-Triassic source rocks such as the P_2l and the third member of Leikoupo Formation (T_2l^3) in the central region Sichuan Basin (CRSB) (Yu, 2022). In prior research regarding the gas-source identification in the CRSB, the emphasis has been placed on the utilization of natural gas compositions, carbon and hydrogen isotopes of gas components, and biomarker indexes of reservoir bitumen. Nevertheless, the indicator parameters of the LHs associated with natural gas are yet to be researched.

Although the content of LHs compounds associated with natural gas is low, their geochemical characteristics play an important role in determining the genetic types of natural gas, gas-source correlation, and secondary transformation (Thompson, 1983; Hu et al., 2010). This paper provides data on the LHs components and its individual carbon isotopes. Combining with the data of natural gas components and the carbon and hydrogen isotopes of each component, a systematic analysis of the natural gas characteristics of T_2l^1 and T_2j^2 in the Triassic System of the MX gas field was carried out. The origin of natural gas in the marine carbonate rock strata of the MX gas field

in the CRSB were discussed, providing a basis for the subsequent exploration of the marine natural gas-rich area in the MX region.

2 Geological setting

The Sichuan Basin is located on the northwestern margin of the Yangtze Platform. It is a superimposed basin that has experienced multiple tectonic movements. The multiple tectonic-sedimentary cycles are related to the opening and closing evolution of the Tethys Ocean. The differentiation period of the marine craton can be divided into three stages, the Sinian-Silurian is the development period of the marine craton fault-depression basin (Ma et al., 2018), the Carboniferous-Middle Triassic is the period of the marine craton depression basin, and the Late Triassic-Cenozoic is the foreland basin period. During the multi-stage tectonic evolution, multiple marine strata have developed, including multiple source rock strata. From the oldest to the youngest, the strata are the Lower Sinian Doushantuo Formation (Z_1ds), the Lower Cambrian Qiongzhusi Formation (E_1q), the Upper Ordovician Wufeng Formation-Lower Silurian Longmaxi Formation (O_1w-S_1l), the Middle Permian Qixia Formation-Maokou Formation (P_2q-P_2m), the Upper Permian Longtan Formation (Wujiaping Formation) and Dalong Formation (P_3l-P_3d) (Figure 1). The vertical distribution of conventional marine carbonate gas reservoirs is mainly controlled by the source rock strata, forming multiple composite petroleum systems.

At the same time, during the multi-stage tectonic evolution, the tectonic characteristics vary in different blocks of the basin. According to their characteristics and the distribution of oil and gas, six tectonic units can be divided: the high-steep tectonic area in eastern Sichuan, the gentle tectonic area in central Sichuan, the low-steep tectonic area in southern and southwestern Sichuan, the western Sichuan sag tectonic area, and the low-flat tectonic area in northern Sichuan (Jiao et al., 2022). However, in the entire Sichuan Basin, the Ordovician to Carboniferous strata are not well-developed. An approximately east-swest-trending extensional fault-depression basin developed, with a cumulative sediment thickness of less than 200 m. In most areas, the Lower Cambrian and Upper Permian sediments are in direct contact. The Silurian is only distributed in the eastern Sichuan area and gradually pinches out in the CRSB (Figure 2B), with only remnants on the edge of the study area. The Dalong Formation (P_3d) is distributed in the Kaijiang-Liangping trough in the northeastern Sichuan area and contributes little to the CRSB. The thickness of the Sinian Doushantuo Formation (Z_1ds) is 10–30 m, and the thickest part is developed in the area of Quang An-Nanchong-Suining. The P_2q-P_2m source rocks are carbonate rocks with low TOC contents, belonging to secondary source rocks. The Gufeng member of the Maokou Formation has an extremely high TOC (0.5%–31.04%, average = 5.08%, Fu et al., 2021), but it is distributed in the northern part of the basin. Therefore, in the CRSB, the E_1q , P_3l , and T_2l^3 are the three sets of source rocks that mainly contribute to the natural gas in the Triassic marine strata.

The gentle tectonic area in CRSB ranges from Yanting in the north to Neijiang-Leshan in the south. The MX Structure, at the high-position of the eastern segment of the Leshan-Longnyusi Paleo-uplift, is the prime target for hydrocarbon accumulation.

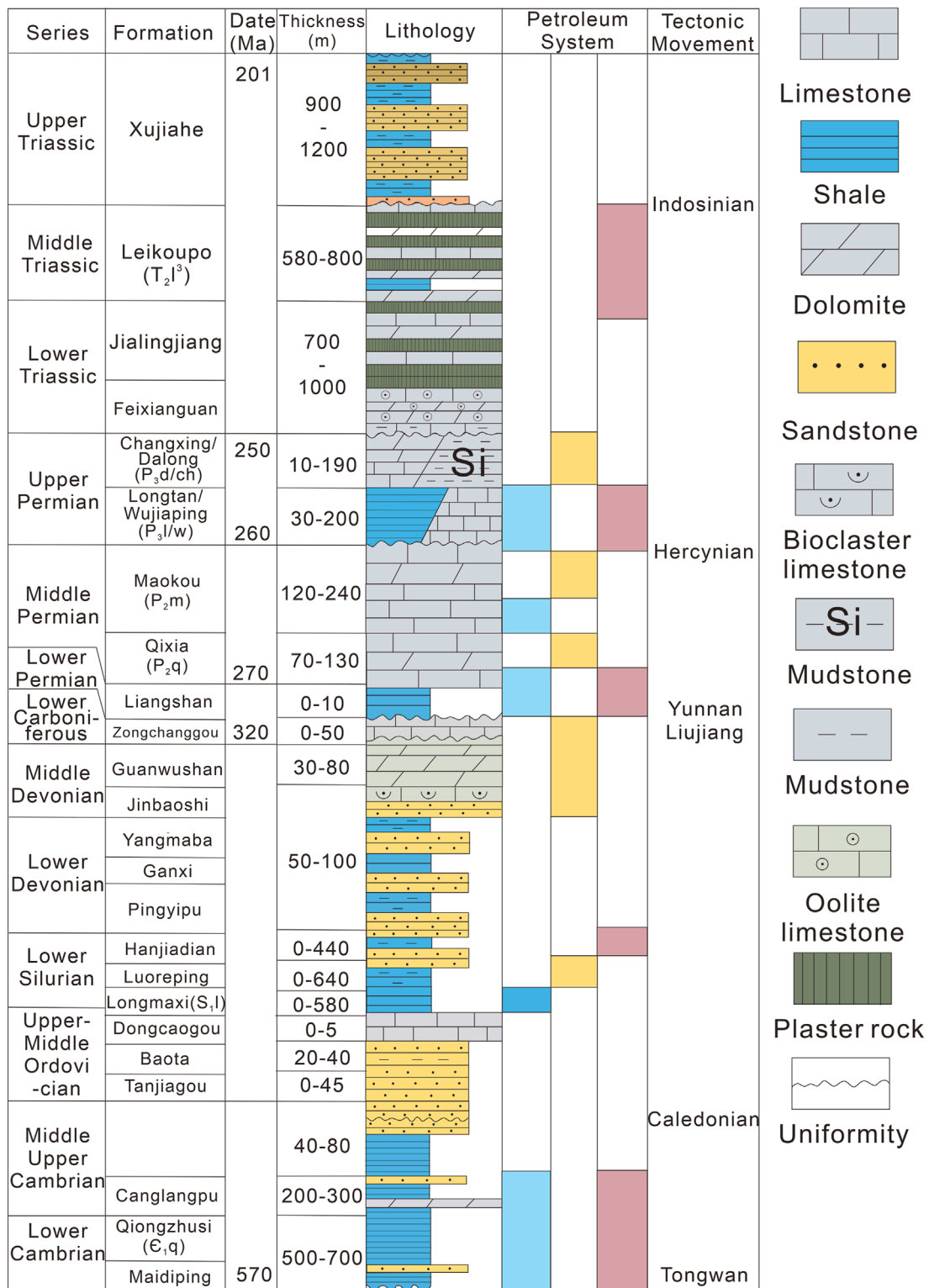
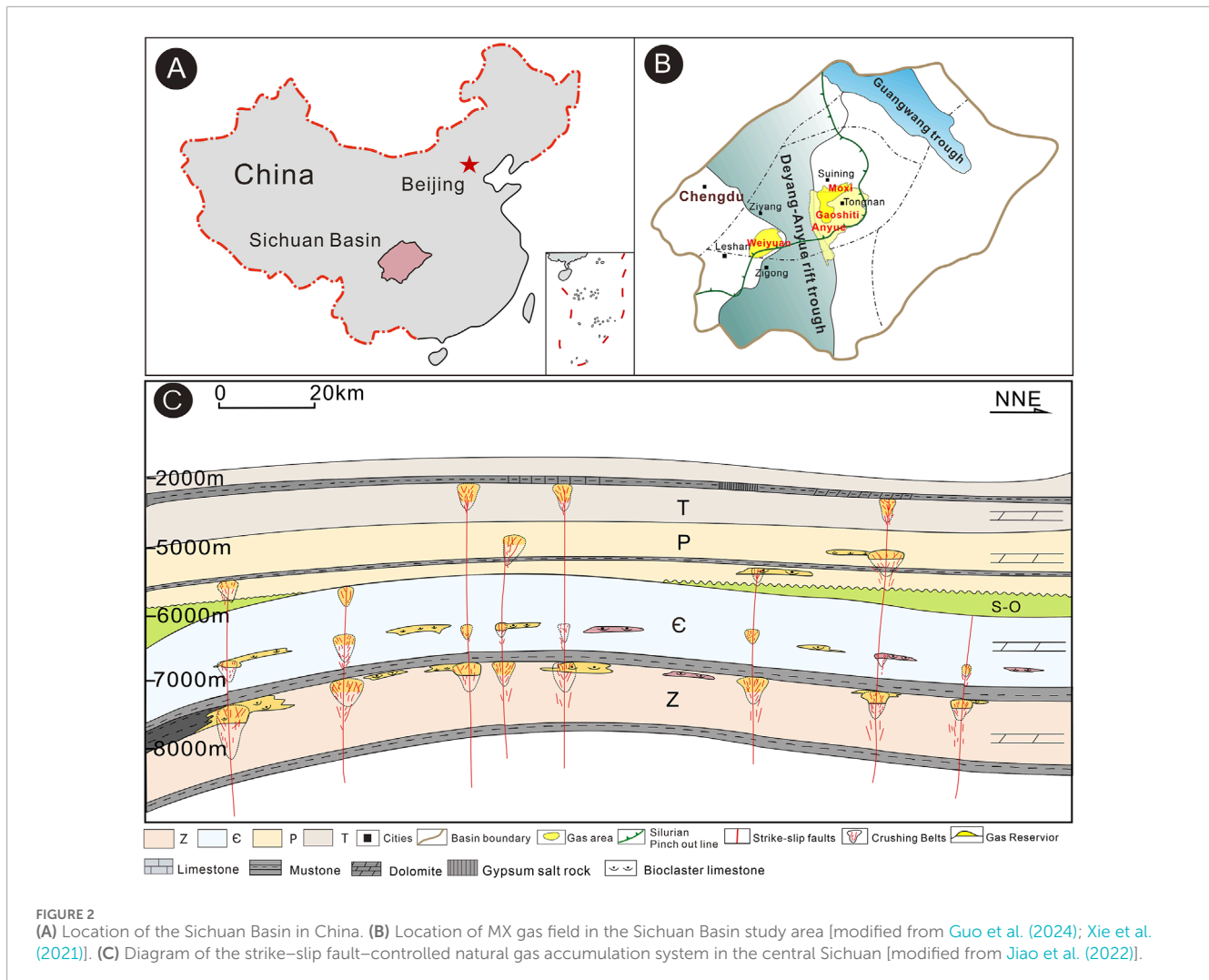


FIGURE 1 Strata column graph of Sichuan Basin and main source rocks are marked in abbreviation [modified from Li et al. (2022); Xie et al. (2020)].

In the Late Sinian, the paleo-uplift began to take shape, while the Cambrian–Ordovician strata were not well-developed. By the late Caledonian at the end of the Silurian, after regional

uplift and subsidence, it was finally formed. During the Indosinian–Himalayan movement, the rapid rise of the Longmen Mountains and the subsequent squeezing transformed the tectonic



pattern and traps. Currently, the Weiyuan gas field (WY) is in the western part of the paleo-uplift's top, and the Anyue (AY) and MX gas fields are in the east. In the CRSB, large-scale strike-slip fault developed in the Sinian-Permian strata, experienced two-stage activities (Ma et al., 2018; Jiao et al., 2022), have laid the groundwork for 3D reservoir exploration (Figure 2C).

3 Samples and experiments

3.1 Samples

A total of 20 natural gas samples were collected. 10 samples were from the T_2^1 and five samples were from the T_2^2 from the Triassic marine carbonate gas reservoirs of the MX gas field in the CRSB. For comparison, five samples from the E_1 in the MX structure of Anyue gas field were also collected. Prior to sampling, a double valve aluminum alloy cylinder (with a volume of 2L) capable of withstanding a gas pressure of 20 Mpa was utilized. The pressure gauge was removed at the wellhead, and the gas cylinder was connected to the wellhead via a hose, both gas valves were opened to flush the cylinder for 3–5 min. Subsequently, one of the

valves was closed to fill the cylinder with gas at a pressure equal to that of the wellhead. During sampling, wells with a pressure ranging from 3 to 10 Mpa and that had been operating normally for an extended period were selected. This was to ensure the success of the light hydrocarbon enrichment experiment.

3.2 Analytical methods

3.2.1 Natural gas analysis

The compositions of natural gas alkane and non-alkane gases, CH_4 and C_2H_6 carbon isotopes, CH_4 hydrogen isotope, and LHs (C_6 – C_7) molecular composition were measured using industry-standard techniques at the PetroChina Research Institute of Petroleum Exploration and Development (Beijing). Gas components were detected by an Agilent 7890B gas chromatograph (GC) with five valves, seven columns, and three detectors (one FID and two TCDs). The FID quantified alkane proportions; the first TCD measured N_2 , CO_2 , and H_2S proportions, with helium as the carrier gas for both. The second TCD, using N_2 as the carrier gas, measured only the He proportion. Carbon isotope compositions were analyzed online with a MAT 253 gas isotope mass spectrometer.

Gaseous hydrocarbons, separated by a PQ capillary column, were transferred by the carrier gas (He) to a combustion furnace, oxidized to CO₂ by CuO at 850°C, and then the converted products were carried to the mass spectrometer for isotope measurement. δ¹³C values were calibrated against the Vienna Pee Dee Belemnite (VPDB) standard, and δD values against the Vienna Standard Mean Ocean Water (VSMOW) standard. Before daily sample analysis, standard samples were measured to ensure instrument stability. The analysis errors for components and δ¹³C were less than 0.3% and 0.5% respectively, and that for δD was less than 5‰.

3.2.2 Light hydrocarbon analysis

The analysis of LHs components was conducted using an Agilent 7890A gas chromatograph (GC) outfitted with a PONA capillary column. At the injection port, the PONA column was coiled repeatedly to create an enrichment loop. Prior to sample injection, this loop was submerged in a liquid-nitrogen cold trap. Ten minutes subsequent to injection, the cold trap was withdrawn, and upon closing the column oven, the analysis was initiated. The column oven temperature was maintained at 30°C for 15 min, then gradually increased to 70°C at a rate of 1.5°C/min, and further elevated to 280°C at a rate of 2.5°C/min. The carbon isotope ratios of LHs (C₆–C₇) were determined *via* GC–C–IRMS, employing the identical temperature programming as that utilized for the determination of LHs components. The detection precisions for LHs components and δ¹³C were ±0.3% and ±0.5‰, respectively.

4 Results

4.1 Chemical composition of natural gas

The molecular compositions and carbon isotopes of 20 gas samples from the Triassic gas reservoirs (T₂^{j2} and T₂^{l1}) in MX gas field and the E₁^l gas samples in MX structure of AY gas field are presented in Table 1. The gas is extremely dry, with a dryness coefficient (C₁/C_n) > 0.99. The gas is predominantly composed of alkane gases, with CH₄ being in an absolutely dominant position, ranging from 96.83% to 99.36% with an average of 96.96%. The C₂H₆ is extremely low (0.2%–0.26%), and the C₃H₈ is lower than that of C₂H₆ (0.01%–0.03%). In certain samples, the C₃H₈ content fell beneath the instrument's detection threshold, precluding the measurement of corresponding values. The content of non-alkane gases is low. The N₂ content ranges from 0.72% to 2.43%, with an average of 1.14%. The CO₂ content is unevenly distributed, ranging from 0.07% to 2.18%, with an average of 0.29%. The H₂S content also varies considerably, ranging from 0% to 2.94%, with an average of 1.36%.

4.2 Stable carbon and hydrogen isotopic composition

Both δ¹³C₁ and δ¹³C₂ values show narrow distribution ranges: δ¹³C₁ ranges from –35.3‰ to –31.4‰ (average = –33.6‰), and δ¹³C₂ from –34.0‰ to –28.6‰ (average = –32.8‰). Owing to the relatively heavy δ¹³C₁ values, carbon isotope reversal (δ¹³C₁ >

δ¹³C₂) occurs in M5, M030–H13 and M91 samples. δD₁ values are generally heavy, varying narrowly from –144‰ to –120‰, with an average of –130‰.

4.3 Molecular composition of C₆–C₇ light hydrocarbons

Table 2 shows the molecular composition and distribution of LHs associated with gas in the MX gas field and MX structure of AY gas field of the CRSB. In the samples, LHs components are characterized by high average contents of cycloalkanes (37.8%) and iso-alkanes (39.5%), while normal alkanes are relatively low, with a maximum of 35% of total C₆–C₇ LHs and an average of 22.6%. For C₇ LHs components, methylcyclohexane (MCH) has the highest average content (55.8%), followed by n-heptane (nC₇, 31.9%) and dimethylcyclopentanes (ΣDMCPs, 14.1%). The Mango coefficient K₁ ratio [(2–MH + 2.3–DMP)/(3–MH + 2.4–DMP)] of T₂^{j2} gas ranges from 1.02 to 1.17, whereas T₂^{l1} shows a wider range, from 0.96 to 1.77. In the E₁^l Fm, low iso-alkane contents precluded K₁ calculation for most samples; the average K₁ of samples M201–1 and M201–2 is 1.16.

4.4 Isotopic characteristics of C₆–C₇ light hydrocarbons

As the gases are over-mature gas and the concentrations of LHs are low, reliable individual carbon isotope data were obtained for only six samples. Meanwhile, over-mature natural gas also suffers from poor separation between adjacent LHs compounds, which affects the detection results of individual carbon isotope values of LHs. The carbon isotope values of seven LHs compounds, namely, 2–MP, 3–MP, nC₆, MCP, CH, nC₇, and MCH, were selected for comparison, as shown in Table 2. Among the seven LHs compounds, δ¹³C_{MCH} is the heaviest, with δ¹³C values ranging from –23.5‰ to –21.3‰ and an average of –22.8‰. The carbon isotope values of normal alkanes, δ¹³C_{nC6} and δ¹³C_{nC7}, are the lightest, with averages of –26.7‰ and –27.0‰ respectively. CH and MCP have the widest distributions of carbon isotope values, showing significant differences among different samples. The δ¹³C_{CH} values range from –26.8‰ to –22.3‰, with an average of –24.4‰, and the δ¹³C_{MCP} values range from –26.3‰ to –23.9‰, with an average of –24.9‰.

Due to the samples being over-mature gas with low LHs concentrations, reliable individual carbon isotope data were available for only six samples. Moreover, over-mature natural gas exhibits poor separation between adjacent LHs compounds, which impacts the carbon isotope detection of individual LHs compounds. As presented in Table 2, the carbon isotope values of seven LHs compounds (2–MP, 3–MP, nC₆, MCP, CH, nC₇, and MCH) were selected for comparison. Among them, δ¹³C_{MCH} is the heaviest, with values from –23.5‰ to –21.3‰ (average = –22.8‰). In contrast, the carbon isotope values of normal alkanes (δ¹³C_{nC6} and δ¹³C_{nC7}) are the lightest, averaging –26.7‰ and –26.9‰ respectively. CH and MCP show the widest carbon-isotope value distributions, varying significantly across samples. The δ¹³C_{CH} values range from –26.8‰ to –22.3‰ (average = –24.4‰), and δ¹³C_{MCP} values from –26.3‰ to –24.0‰ (average = –24.9‰).

TABLE 1 Molecular and stable isotopic compositions of gas from Triassic and Cambrian reservoirs in the MX and AY gas fields.

Well	Fm	Gas pool	Depth/m	Chemical Composition (vol%)						Dryness Coefficient	$\delta^{13}C$ (‰, VPDB)		δD (‰, VSMOW)	
				C ₁	C ₂	C ₃₊	N ₂	CO ₂	H ₂ S		CH ₄	C ₂ H ₆		CH ₄
M005-H9	T ₂ ²	MX gas field	3,190–3,192	99.27	0.20	0.01	0.52	0.00	0.00	0.00	0.9979	-33.9	-34.1	-140
M157	T ₂ ²		3,147–3,160	99.35	0.19	0.01	0.45	0.00	0.00	0.00	0.9980	-34.6	-34.1	-139
MS1	T ₂ ²		3,128–3,180	96.83	0.20	0.01	0.72	2.18	0.06	0.06	0.9978	-34.2	-33.6	-122
MS1-2	T ₂ ²		3,128–3,180	97.06	0.20	0.01	2.43	0.31	0.00	0.00	0.9978	-33.2	-31.9	—
M5	T ₂ ²		3,079–3,132	97.04	0.26	0.03	2.22	0.40	0.05	0.05	0.9970	-33.1	-33.8	—
M030-H13	T ₂ ¹		3,722	97.23	0.18	0.01	1.02	0.13	1.43	1.43	0.9980	-32.9	-33.9	-135
M030-H14	T ₂ ¹		3,670	97.29	0.23	0.01	1.05	0.12	1.30	1.30	0.9976	-35.3	—	-132
M030-H16	T ₂ ¹		3,589	97.45	0.20	0.01	1.00	0.14	1.21	1.21	0.9979	-33.7	-33.5	-138
M030-H17	T ₂ ¹		3,612	97.20	0.19	0.01	1.03	0.13	1.45	1.45	0.9980	-33.5	-32.6	-138
M004-H9	T ₂ ¹		3,717	95.89	0.20	0.01	1.18	0.17	2.56	2.56	0.9978	-34.9	-32.9	-144
M004-H10	T ₂ ¹		3,270	96.34	0.19	0.02	1.13	0.15	2.16	2.16	0.9978	-34.9	-33.5	-144
M91	T ₂ ¹		2,676	96.62	0.19	0.00	1.03	0.12	2.03	2.03	0.9980	-32.9	-33.1	-123
M89	T ₂ ¹	2,723	95.46	0.19	0.00	1.23	0.16	2.94	2.94	0.9980	-33.8	-33.2	-124	
M017-H3	T ₂ ¹	3,200	96.48	0.20	0.00	1.05	0.14	2.12	2.12	0.9980	-33.9	-33.6	-124	
M032-H2	T ₂ ¹	3,431	96.23	0.24	0.00	1.19	0.15	2.17	2.17	0.9975	-33.7	-33.5	-120	
M201-1	E ₁ /I	4,575	95.91	0.13	0.01	0.80	2.83	0.32	0.32	0.9985	-33.1	-33.0	-133	
M12	E ₁ /I	4,640	95.98	0.13	0.01	0.73	2.53	0.62	0.62	0.9985	-33.4	-33.4	-134	
M009-X1	E ₁ /I	4,750	96.50	0.14	0.01	0.78	2.07	0.50	0.50	0.9984	-33.0	-32.8	-137	
M8	E ₁ /I	4,660	96.80	0.14	0.01	0.69	1.76	0.60	0.60	0.9985	-32.4	-32.3	-133	
M201-2	E ₁ /I	4,574–4,608	96.45	0.14	0.00	0.62	2.08	0.70	0.70	0.9985	-33.5	-33.3	-122	

*Dryness Coefficient = C₁/C_n.
 ***— represent "not available".

TABLE 2 Relative contents, main component parameters, and isotope ratios of C₆–C₇ LHs with natural gases from the MX and AY gas fields.

Well	Fm	Gas pool	Depth/m	C ₆ –7-alkanes/GC area (%)			C ₇ /GC area (%)			(2–MH+2.3–DMP)/nC ₇			(3–MH+2.4–DMP)/nC ₇			K ₁	δ ¹³ C (‰,VPDB)						
				Iso	Normal	Cyc	MCH	nC ₇	∑DMCPs	MCH	nC ₇	∑DMCPs	(2–MH+2.3–DMP)/nC ₇	(3–MH+2.4–DMP)/nC ₇	2–MP		3–MP	nC ₆	MCP	CH	nC ₇	MCH	
M005-H9	T ₂ J ²	MX gas field	3,190–3,192	21.53	9.59	68.88	28.01	61.99	10.00	1.03	0.93	1.11	–	–	–	–	–	–	–	–			
M157	T ₂ J ²		3,147–3,160	40.05	10.29	49.66	38.93	38.40	22.67	1.37	1.33	1.02	–	–	–	–	–	–	–	–			
MS1	T ₂ J ²		3,128–3,180	31.32	20.97	47.71	47.98	43.77	8.25	0.69	0.58	1.17	–27.8	–28.1	–28.4	–26.8	–24.2	–29.1	–23.5	–			
MS1-2	T ₂ J ²		3,128–3,180	33.38	22.29	44.32	51.13	40.70	8.16	0.65	0.59	1.11	–	–	–	–	–	–	–	–			
M5	T ₂ J ²		3,079–3,132	38.76	9.26	51.98	35.74	38.68	25.59	2.06	1.37	1.50	–	–	–	–	–	–	–	–			
M030-	T ₂ J ¹		3,722	52.39	17.05	30.56	61.37	27.00	11.63	1.31	1.37	0.96	–	–	–	–	–	–	–	–			
M030-H14	T ₂ J ¹		3,670	42.19	24.54	33.27	62.15	30.99	6.86	0.77	0.69	1.11	–	–	–	–	–	–	–	–			
M030-H16	T ₂ J ¹		3,589	44.30	32.98	22.72	69.55	20.45	10.00	0.59	0.54	1.10	–	–	–	–	–	–	–	–			
M030-H17	T ₂ J ¹		3,612	36.86	33.13	30.01	57.60	24.70	17.70	0.44	0.43	1.02	–	–	–	–	–	–	–	–			
M004-H9	T ₂ J ¹		3,717	42.07	33.01	24.92	66.32	22.01	11.66	0.63	0.43	1.45	–	–	–	–	–	–	–	–			
M004-H10	T ₂ J ¹		3,270	40.38	34.18	25.44	66.03	22.53	11.44	0.57	0.41	1.38	–	–	–	–	–	–	–	–			
M91	T ₂ J ¹		2,676	33.34	22.25	44.41	51.06	40.79	8.15	0.65	0.59	1.11	–24.1	–24.6	–26.6	–24.2	–	–26.4	–21.3	–			
M89	T ₂ J ¹		2,723	51.30	33.46	15.24	76.25	13.71	10.03	0.65	0.48	1.36	–24.5	–24.6	–27.0	–	–24.8	–	–	–			
M017-H3	T ₂ J ¹		3,200	56.79	30.11	13.10	77.83	11.73	10.43	0.75	0.61	1.24	–22.2	–21.9	–24.8	–22.3	–25.0	–26.4	–23.5	–			
M032-H2	T ₂ J ¹		3,431	46.62	35.79	17.59	73.93	15.78	10.29	0.58	0.40	1.45	–24.3	–24.7	–27.0	–23.7	–26.3	–25.6	–23.4	–			

(Continued on the following page)

TABLE 2 (Continued) Relative contents, main component parameters, and isotope ratios of C₆–C₇ LHs with natural gases from the MX and AY gas fields.

Well	Fm	Gas pool	Depth/m	C ₆ –alkanes/GC area (%)			C ₇ /GC area (%)			C ₇ /GC area (%)			K ₁	δ ¹³ C (‰, VPDB)					
				Iso	Normal	Cyc	MCH	nC ₇	ΣDMCPs	(2–MH+2.3–DMP)/nC ₇	(3–MH+2.4–DMP)/nC ₇	2–MP		3–MP	nC ₆	MCP	CH	nC ₇	MCH
M201-1	E ₁ l	AY gas field (MX structure)	4,575	31.66	32.08	36.26	54.13	30.80	15.07	0.44	0.42	1.05	–	–	–	–	–		
M12	E ₁ l		4,640	41.99	13.29	44.72	52.43	42.41	5.16	0.79	1.02	0.77	–	–	–	–	–		
M009-X1	E ₁ l		4,750	45.37	11.30	43.33	53.63	41.01	5.36	1.03	1.94	0.53	–	–	–	–	–		
M8	E ₁ l		4,660	38.03	8.78	53.19	36.60	41.59	21.82	1.28	2.65	0.48	–	–	–	–	–		
M201-2	E ₁ l		4,574–4,608	36.91	24.16	38.93	53.76	34.27	11.98	0.60	0.47	1.27	–24.6	–24.7	–26.7	–23.9	–27.3	–23.4	

*2–MH, 2–methylpentane; 3–MH, 3–methylpentane; 2,3–DMP, 2,3–dimethylpentane; 2,4–DMP, 2,4–dimethylpentane; nC₆, hexane; MCH, methylcyclopentane; CH, cyclohexane; nC₇, heptane; MCH, methylcyclohexane.
 **K₁ = (2–MH + 2.3–DMP)/(3–MH + 2.4–DMP).
 ***“–” represent “not available”.

5 Discussion

5.1 Genetic identification of gas

On the δ¹³C₁ vs C₁/C₂+C₃ gas genetic diagram proposed by (Milkov et al., 2020) and the modified Bernard diagram (Figure 3A; Bernard et al., 1978), the gas samples mainly represent late–mature thermogenic gases. The δ¹³C₂₋₁ vs δ¹³C₁ plot (Figure 3B) also shows the characteristics of late–mature thermogenic gases (Milkov, 2021). Numerous case studies have indicated that the δ¹³C₁ in natural gas is primarily influenced by maturity (Stahl and Carey, 1975; Schoell, 1980; Dai, 1993). In contrast, the δ¹³C values of heavier hydrocarbons such as C₂H₆ and C₃H₈ are less affected by maturity and mainly reflect the organic matter type of source rock. Based on the linear relationship between vitrinite reflectance (Ro) and the δ¹³C₁ of natural gas, empirical formulas for its variation have been deduced. Chen et al. (2021) comprehensively evaluated these formulas and pointed out that previous formulas often showed deviations when determining the maturity of gas source rocks. By combining actual geological conditions and a large amount of measured gas data, they revised the relationship between the δ¹³C₁ in oil–type gas and coal–derived gas and the vitrinite reflectance (Ro) of the source rock. The revised formulas are, for oil–type gas, δ¹³C₁ = 25lgRo–42.5; for coal–derived gas, δ¹³C₁ = 25lgRo–37.5. In this study, the above formulas were applied to estimate the maturity of gas source rocks in each production layer in the MX area of CRSB. The estimated maturities of gas from the Triassic and the E₁l in the MX area are as follows, the maturity of T₂j² gas ranges from 2.34% to 2.38% (average = 2.36%), that of T₂l¹ gas ranges from 1.94% to 2.43% (average = 2.21%), and that of the E₁l gas ranges from 2.31% to 2.54% (average = 2.38%). According to the classification criteria for the thermal evolution stages of organic matter in source rocks, the gas source rocks of the Triassic and E₁l in the MX area are mainly in the over–mature stage, with the gas maturities of T₂j² and E₁l being slightly higher than that of T₂l¹. Correspondingly, the same conclusion can be drawn from the δ¹³C₁ vs δD₁ diagram (Figure 3D).

Based on the type of organic matter in source rocks, thermogenic gases can be classified into oil–type gas and coal–derived gas. The former is mainly generated from sapropelic organic matter, while the latter is primarily produced from humic organic matter (Dai et al., 1992). The data points of the samples fall within the range of shale–sourced rather than coal–sourced gases in the Milkov diagram (Figure 3B; Milkov, 2021) and follow the trend of gases generated from Type II kerogen in the modified Bernard diagram (Figure 3A; Bernard et al., 1978), exhibiting typical characteristics of oil–type gas. This shows significant differences from the coal–derived gas in the T₂x in the Zhongba area and the natural gas in the Feixianguan Formation sourced from the P₃l in the Longgang area of the Sichuan Basin. The hydrogen isotope composition of natural gas is influenced by the organic matter in the source rock, thermal maturity, and the conditions of the aqueous medium, and thus is commonly used to identify the origin of natural gas (Dai et al., 2012; Wang et al., 2015). Generally, the δD₁ values of oil–type gas are higher than those of coal–derived gas with the same or similar δ¹³C₁ values. The δD₁ values of T₂j² and T₂l¹ gas are generally heavier than –140‰, ranging from –144‰ to –120‰ (average = –131‰). All samples show the characteristics of oil–type gas in the δ¹³C₁ vs δD₁ diagram (Figure 3D), and there

TABLE 3 Geochemical data for the components and stable carbon and hydrogen isotopes of natural gases for correlation in the Sichuan Basin.

Gas field	Well	Fm	Depth /m	Molecular compositions/%					Dryness coefficient	$\delta^{13}C/\text{‰}$, VPDB			References		
				CH ₄	C ₂ H ₆	C ₃₊	CO ₂	N ₂		H ₂ S	CH ₄	C ₂ H ₆		C ₁ -C ₂	$\delta D/\text{‰}$, VSMOW
GFC	Feng8	C ₂ hl	5,194	94.36	1.06	0.10	1.22	3.26	0.08	0.9879	-33.8	-37.3	3.5	-122	Liu et al. (2014)
	Tiandong9	C ₂ hl	4,588	95.82	1.27	0.42	1.67	0.79	0.04	0.9827	-34.6	-38.0	3.4	-122	
SPC	Tiandong93	C ₂ hl	4,977	95.46	0.88	0.09	2.59	0.98	0.01	0.9899	-35.1	-37.4	2.3	—	Liu et al. (2014)
	Yuedong1	C ₂ hl	5,171	96.66	0.84	0.07	1.76	0.67	0.05	0.9907	-33.4	-37.3	3.9	-108	
WLH	W094	C ₂ hl	3,850	97.05	0.88	0.11	1.44	0.52	0.14	0.9899	-32.4	-36.9	4.5	-116	Liu et al. (2014)
	Xiang22	C ₂ hl	2,660	98.05	0.88	0.12	0.58	0.37	—	0.9899	-33.0	-35.1	—	—	
JN	Jian32-1	C ₂ hl	3,744	92.72	1.24	0.34	1.00	4.58	—	0.9832	-37.0	-41.8	—	-126	Liu et al. (2014)
	Tiandong51	C ₂ hl	5,035	96.41	0.95	0.09	1.78	0.76	0.12	0.9893	-31.9	-37.2	5.3	-123	
SGP	Guang19	C ₂ hl	4,388	97.20	0.73	0.05	1.35	0.67	0.42	0.9920	-31.8	-36.2	4.4	-118	Liu et al. (2014)
	Qili53	C ₂ hl	4,806	97.39	0.61	0.02	1.55	0.43	0.40	0.9936	-31.9	-34.6	2.7	-123	
TMC	Oil28	C ₂ hl	5,046	96.17	0.66	0.03	2.00	1.61	0.34	0.9929	-31.3	—	—	-117	Liu et al. (2014)
	Tieshan4	C ₂ hl	4,035	97.47	0.19	0.01	0.87	0.68	0.77	0.9980	-30.8	—	—	-116	
ZB	Z19	T ₃ x ²	2,602	90.36	5.81	2.20	0.45	0.63	—	0.9190	-35.0	-24.0	-11.0	-170	Hu et al. (2013)
	Z34	T ₃ x ²	2,408	90.80	5.70	2.07	0.48	0.53	—	0.920	-35.4	-24.5	-10.9	-170	
ZB	Z36	T ₃ x ²	2,628	90.90	5.75	2.15	0.52	0.21	—	0.9200	-35.4	-24.4	-11.0	-171	Hu et al. (2013)
	Z44	T ₃ x ²	2,510	90.19	5.79	2.23	0.47	0.91	—	0.9180	-35.0	-24.0	-11.0	-171	
ZB	Z63	T ₃ x ²	2,366	91.00	5.75	2.09	0.46	0.28	—	0.9210	-35.5	-24.4	-11.1	-170	Hu et al. (2013)
	Z2	T ₃ x ²	2,578	90.53	5.75	2.14	0.54	0.46	—	0.9200	-35.3	-24.3	-11.0	-171	
ZB	Z16	T ₃ x ²	2,446	89.80	6.10	2.46	0.56	0.49	—	0.9130	-35.6	-24.3	-11.3	-171	Hu et al. (2013)
	Z2	T ₃ x ²	2,400	90.82	5.77	2.11	0.47	0.27	—	0.9200	-35.5	-24.3	-11.2	-170	
ZB	Z29	T ₃ x ²	2,268-2,361	87.86	6.53	3.53	0.39	0.28	—	0.8970	-34.8	-24.8	-10.0	-171	Hu et al. (2013)
	Z39	T ₃ x ²	2,422	87.82	6.36	5.02	0.32	0.03	—	0.8850	-36.9	-25.6	-11.3	-173	

(Continued on the following page)

TABLE 3 (Continued) Geochemical data for the components and stable carbon and hydrogen isotopes of natural gases for correlation in the Sichuan Basin.

Gas field	Well	Fm	Depth/m	Molecular compositions/%					Dryness coefficient				$\delta^{13}C/\text{‰}$, VPDB			References	
				CH ₄	C ₂ H ₆	C ₃₊	CO ₂	N ₂	H ₂ S	CH ₄	C ₂ H ₆	C ₁ -C ₂	CH ₄	C ₁ -C ₂	CH ₄		
HWC	H2	P ₂ m	—	97.41	0.10	0.01	1.56	0.54	0.39	0.9990	0.9990	0.9990	-35.7	-33.4	-2.3	-136	Guo et al. (2024)
	H6	P ₂ m	—	97.85	0.60	0.06	0.06	1.38	0.05	0.9930	0.9930	0.9930	-34.6	-32.5	-2.1	-137	
	H3	P ₂ m	—	98.63	0.84	0.09	0.07	0.37	0.00	0.9910	0.9910	0.9910	-35.5	-33.4	-2.1	-135	
WJB	WT1	P ₂ m	—	98.59	0.18	0.01	0	1.22	0.00	0.9980	0.9980	0.9980	-35.5	-35.2	—	—	
	LG9	—	—	91.19	5.11	2.41	0.85	0.44	0.00	0.9238	0.9238	0.9238	-31.2	-26.3	-4.9	-143	
LG	LG160	—	—	95.65	2.17	0.4	1.57	0.18	0.00	0.9738	0.9738	0.9738	-29.0	-27.6	-1.4	-190	Deng et al. (2018)
	LG001-3	T ₁ f ³	6,348-6,365	96.32	1.54	0.34	1.36	0.40	0.00	0.9809	0.9809	0.9809	-29.3	-23.5	-5.8	-154	
	LG001-1	T ₁ f ³	—	95.38	0.07	0.01	3.87	0.67	0.00	0.9992	0.9992	0.9992	-31.2	-27.3	-3.9	-141	
	LG001-6	T ₁ f ³	—	95.25	0.2	0.03	3.9	0.62	0.00	0.9976	0.9976	0.9976	-29.0	-26.4	-2.6	-184	
	LG001-7	T ₁ f ³	—	94.39	0.06	0.01	2.49	1.27	1.75	0.9993	0.9993	0.9993	-31.3	-26.6	-4.7	-128	
	LG001-2	P ₂ dt	6,261-6,828	92.35	0.09	0.00	5.67	0.28	1.61	0.9990	0.9990	0.9990	-31.6	-27.3	-4.3	-128	
	LG001-8-1	P ₂ dt	6,261-6,364	96.26	0.12	0.11	3.13	0.38	0.00	0.9976	0.9976	0.9976	-31.6	-27.0	-4.6	-124	
	LG1	T ₁ f ³	6,055-6,124	95.41	0.08	0.00	3.89	0.62	0.00	0.9992	0.9992	0.9992	-30.6	-24.3	-6.3	-150	
	LG001-30	P ₂ dt	6,238-6,346	88.40	0.06	0.1	7.68	0.39	3.37	0.9982	0.9982	0.9982	-30.5	-26.5	-4.0	-144	
	LG001-32	P ₂ dt	4,075-6,075	88.99	0.06	0.00	6.59	0.31	4.05	0.9993	0.9993	0.9993	-31.4	-25.2	-6.2	-136	
	LG001-26	P ₂ dt	6,480	88.42	0.06	0.00	7.39	1.97	2.16	0.9993	0.9993	0.9993	-30.0	-23.9	-6.1	-148	
	LG26	T ₁ f ³	5,536-5,796	93.77	0.06	1.39	4.63	0.00	0.15	0.9848	0.9848	0.9848	-30.9	-26.3	-4.6	-128	
	LG6	T ₁ f ³	4,781-4,889	94.13	0.06	0.01	4.34	0.57	0.89	0.9993	0.9993	0.9993	-31.4	-25.6	-5.8	-139	
	LG27	T ₁ f ³	5,170	90.71	0.08	0.53	6.32	0.51	1.85	0.9933	0.9933	0.9933	-31.4	—	-31.4	-130	
LG001-28	P ₂ dt	—	91.22	0.06	0.01	7.8	0.21	0.70	0.9992	0.9992	0.9992	-30.8	-26.4	-4.4	-151		

(Continued on the following page)

TABLE 3 (Continued) Geochemical data for the components and stable carbon and hydrogen isotopes of natural gases for correlation in the Sichuan Basin.

Gas field	Well	Fm	Depth/m	Molecular compositions/%					Dryness coefficient			$\delta^{13}C_i/\%$, VPDB			References
				CH ₄	C ₂ H ₆	C ₃₊	CO ₂	N ₂	H ₂ S	CH ₄	C ₂ H ₆	C ₁ -C ₂	$\delta D_i/\%$, VSMOW		
	MX21	E ₁ l	—	95.21	0.27	0.00	3.93	0.28	0.16	0.9972	-33.5	-34.9	1.4	-132	
	MX201	E ₁ l	—	95.91	0.13	0.00	2.83	0.78	0.51	0.9986	-33.1	-33.0	-0.1	-133	
	MX202	E ₁ l	—	95.48	0.15	0.00	2.89	0.63	0.84	0.9984	-34.7	-35.3	0.6	-132	
	MX204	E ₁ l	—	96.63	0.13	0.00	2.06	0.71	0.40	0.9987	-32.6	-32.4	-0.2	-134	
	MX205	E ₁ l	—	95.30	0.2	0.00	3.18	0.42	0.73	0.9979	-33.2	-34.8	1.6	-132	
	MX008-HI	E ₁ l	—	95.15	0.14	0.00	3.34	0.70	0.52	0.9985	-32.2	-33.3	1.1	-136	
	MX009-XI	E ₁ l	—	96.50	0.14	0.00	2.37	0.67	0.61	0.9986	-33.0	-33.3	0.3	-137	
	MX13	E ₁ l	—	95.44	0.13	0.00	1.65	0.70	0.50	0.9986	-32.7	-33.0	0.3	-132	

*Dryness Coefficient = C₁/C₂;
 ***— represent "not available".

is a positive correlation between δD_1 and $\delta^{13}C_1$, indicating that as gas maturity increases, δD_1 is significantly affected and shows a gradually increasing trend. The salinity of water during source rock formation affects the hydrogen isotope composition of natural gas. Compared with fresh water, saltwater is rich in deuterium (D), which usually results in higher δD_1 values in natural gas generated in such environments (Schoell, 1980; Wang et al., 2015; Ni et al., 2019). The samples can be roughly divided into two parts based on δD_1 values, gas with $\delta D_1 > -132\%$ mainly comes from T₂², while gas with $\delta D_1 < -132\%$ is from E₁l and T₂¹. Considering that the source rocks in these areas are generally in the high to over-mature stage, the increase in water salinity during source rock deposition rather than maturity may be the reason for the higher δD_1 values in gas. The wide distribution of data points for T₂¹ gas may be due to the complexity of the gas source rocks or the existence of mixing effect.

Given that the C₃H₆ content in certain samples is below the instrument's detection limit, registering as 0%, the ln(C₂/C₃) vs ln(C₁/C₂) plot is inapplicable for differentiating kerogen-cracking gas from oil-cracking gas in this study. On the C₁/C_n vs $\delta^{13}C_1$ diagram (Figure 3C), the $\delta^{13}C_1$ values of all samples are less than -30‰, indicating that they belong to the category of oil-cracking gas. These samples can be compared with natural gas from other regions that has been confirmed as oil-cracking gas, such as the Z₂dn gas in the GST-MX area and the E₁l gas in the MX area (Wei et al., 2015), the C₂hl gas in eastern Sichuan (Liu et al., 2014), and the P₂m gas in the HWC and WJB gas fields in northwestern Sichuan (Guo et al., 2024). They differ from the coal-derived gas in the P₂ch-T₁³ Fms in the LG gas field that displays characteristics of kerogen-cracking gas. In addition, the relative contents of non-hydrocarbon gases CO₂ and N₂ can also be used to identify the formation pathways of natural gas (Liu et al., 2012), which is related to the high content of nitrogen-containing compounds in argillaceous source rocks. During the thermal evolution of argillaceous source rocks, denitrification occurs, resulting in a higher N₂ content in kerogen-cracking gas than in oil-cracking gas. According to the CO₂-N₂ relationship diagram proposed by Li et al. (2022), the boundary of the N₂ content between oil-cracking gas and kerogen-cracking gas in the Sichuan Basin is approximately 4%. Samples with an N₂ content higher than 4% in natural gas can generally be considered as kerogen-cracking gas. Therefore, all the natural gas in the Triassic marine strata of the MX area is oil-cracking gas. However, according to the LHs discrimination diagrams (Figures 4A, B), most T₁¹ samples have relatively low MCH/nC₇ ratios, and the data points fall into the mixed-gas region of oil-cracking gas and kerogen-cracking gas. It is believed that the mixing of gas with a relatively high MCH content in the gas of the T₁¹ causes deviations in the results.

On the $\delta^{13}C_{2-1}$ vs $\delta^{13}C_1$ plot (Figure 3B), some gases from the Triassic and the E₁l Fm are located in the reversal region ($\delta^{13}C_1 > \delta^{13}C_2$). Considering the distribution of several potential source rocks (Figure 1) and the high maturity of the natural gas, there are several reasonable explanations for the observed phenomenon of $\delta^{13}C_1 > \delta^{13}C_2$. (1) Mixing of hydrocarbon gases generated by thermal cracking of oils from different source rocks. In the CRSB, there are three potential source rocks, the E₁q marine shale, the Upper Permian marine shale, mudstone, and carbonate rocks of P₂l, and the T₂³ marine shale (Figure 1). These source rocks are mainly composed of sapropelic organic matter and may thus

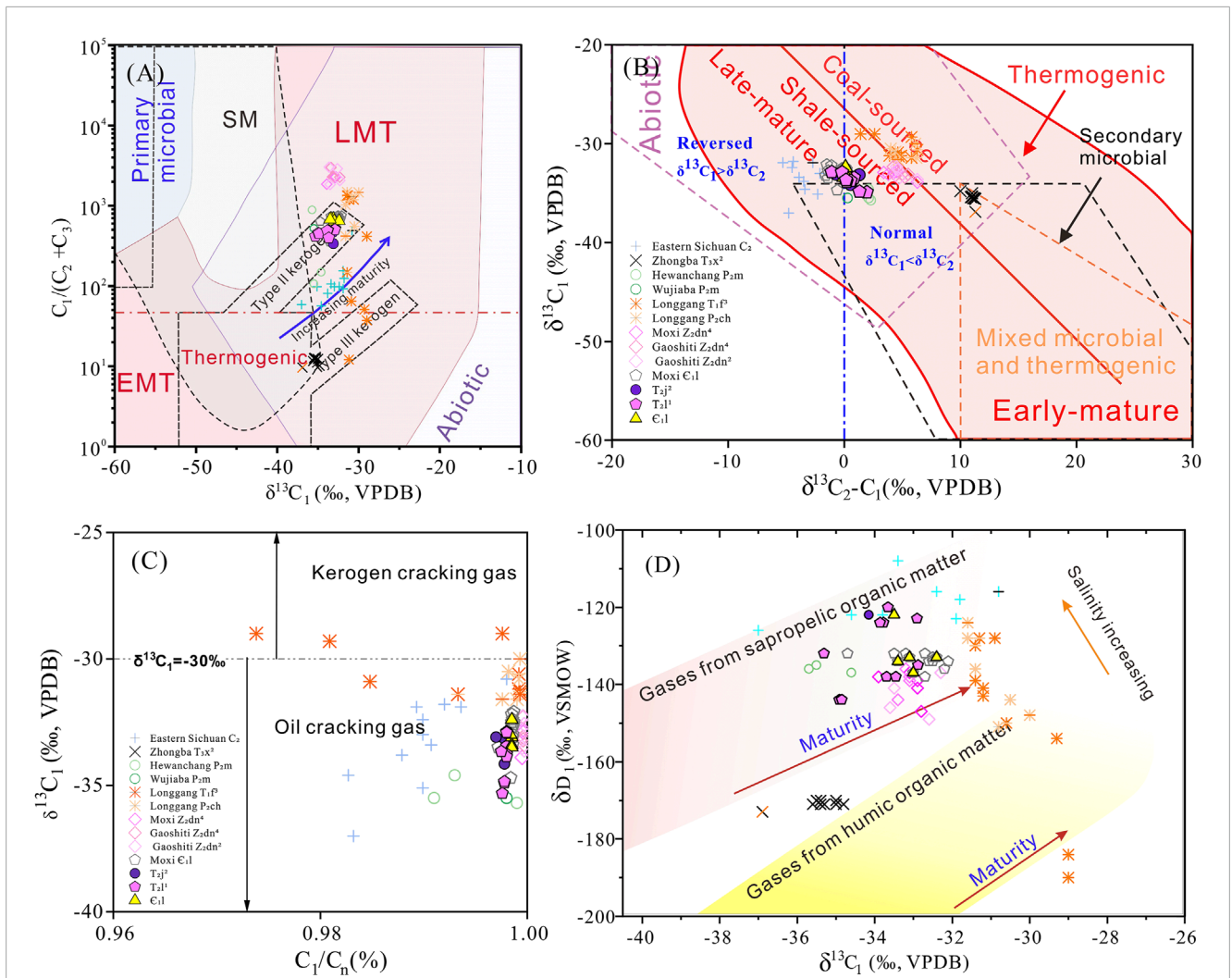


FIGURE 3 Relationship diagram between (A) $\delta^{13}C_1$ vs. $C_1/(C_2+C_3)$. Abbreviations: SM—secondary microbial, EMT—early mature thermogenic gas, LMT—late mature thermogenic gas [adapted from Bernard et al. (1978); Milkov et al. (2020)], (B) $\Delta\delta^{13}C_2-\delta^{13}C_1$ vs $\delta^{13}C_1$ [adapted from Milkov (2021)], (C) C_1/C_n vs. $\delta^{13}C_1$. [adapted from Clayton (1991)] and (D) $\delta^{13}C_1$ vs δD_1 [adapted from Wang et al. (2015)] of T_2j^2, T_2l^1 gas in the MX gas field and E_1l gas in the AY gas field, Sichuan Basin (Data source same as Table 3).

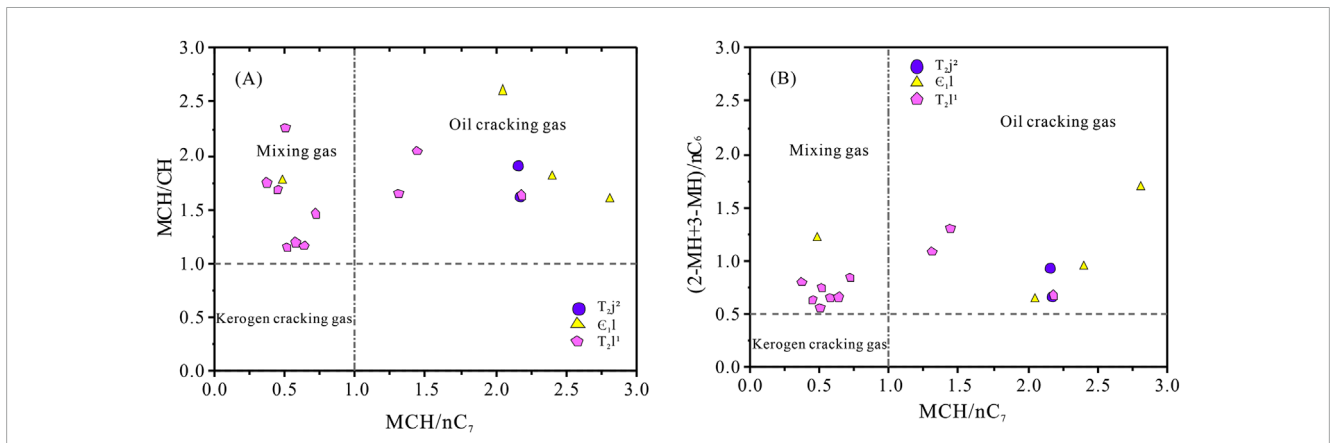


FIGURE 4 Cross-plot of MCH/nC_7 versus MCH/CH (A) and MCH/nC_7 versus $(2-MH+3-MH)/nC_6$ (B) of T_2j^2, T_2l^1 gas in the MX gas field and E_1l gas in the AY gas field [modified from Hu et al. (2005)].

contribute to the accumulated oils that generate secondary–cracking gases. Although existing data suggest that the accumulated oils in the T_2l^1 gas reservoir are mainly sourced from the Upper Permian source rocks (Wang et al., 1998), the contribution of other source rocks (such as the Lower Triassic marine shale) cannot be excluded. (2) Mixing of secondary–cracking gases and primary–cracking gases. As mentioned earlier, all samples are secondary–cracking gases (Figure 3C), while this explanation is not applicable to the Triassic gas in CRSB. (3) Mixing of gases from thermal cracking of previously–accumulated oils at different maturity levels may occur within the reservoir. However, Triassic dry gas reservoirs did not evolve from paleo oil reservoirs within the stratigraphic system. Thus, the gases likely accumulated instantaneously. Nevertheless, it cannot be ruled out that the mixture of gases generated by thermal cracking of accumulated oils at different maturity levels in the Lower Cambrian migrated upward and retained their reversed characteristics.

5.2 Gas–source correlation

The distribution of various sets of source rocks has been discussed in the geological setting. The E_1q Fm, P_2l Fm and T_2l^3 Fm are three sets of source rocks that may contribute to the natural gas in the Triassic marine strata. The E_1q source rock is controlled by the Deyang–Anyue rift trough and has a widespread distribution (Figure 2B). It has strong hydrocarbon – generating potential and is one of the highest–quality source rocks in the Sichuan Basin. Its gas–generation intensity reaches 20×10^8 – 200×10^8 m^3/km^2 (Zhang et al., 2024). However, the gypsum layers developed in the overlying Cambrian Gaotai Formation (E_1g) and E_1l are distributed in the eastern and southern Sichuan Basin, and they do not play a capping role for the hydrocarbon–generation of the E_1q in the MX area of CRSB (Xu et al., 2016). In addition, the multi–stage strike–slip faults developed in the CRSB serve as “highways” for oil and gas migration. These faults have been active in multiple stages from the Sinian to the Cretaceous. The Indosinian period was the main stage of oil – generation from the Lower Cambrian shale, and traps along the migration pathways may have captured the oil and gas generated in historical periods (Shuai et al., 2022; Lu et al., 2024).

The P_2l source rock has sedimentary centers in both central and northeastern Sichuan Basin. The maximum sedimentary thickness can reach 120–140 m. The superior source rock conditions have laid a material foundation for hydrocarbon generation in the central Sichuan region. However, according to the burial history of Well GS 17, the P_2l source rock in the CRSB entered the high–maturity stage (geo–temperature > 180°C) during the Cretaceous period (Figure 5; Yang et al., 2020). Subsequently, under the influence of the uplift of the Indosinian movement, the temperature dropped rapidly. Therefore, it did not experience a large scale dry gas generation stage in history. As can be seen from the hydrocarbon–expulsion intensity map of the P_2l Fm at the end of the Triassic, the hydrocarbon–expulsion amount is less than 50×10^8 t/km^2 south of Suining in the CRSB (Zhang et al., 2022).

As for the Triassic T_2l^3 marl, it is a set of lagoonal facies source rocks explored in recent years. The average TOC of the T_2l^3 cuttings in Well CT1 is 0.77%, the organic matter type is Type II, and the measured Ro is 1.59–1.63%, indicating a high mature stage (Yu, 2022; Wang et al.,

2023). Currently, only the self–generated and self–stored reservoir of the T_2l^3 marl in Well CT1 has been discovered, and no contribution to conventional gas reservoirs has been found yet.

The T_2j^2 and T_2l^1 gases are oil–type gases and specifically oil–cracking gases. The $\delta^{13}C_{\text{kerogen}}$ of P_2l ranges from –24‰ to –23‰, and the organic matter type is II₂–III (Huang et al., 2024). According to the carbon isotope fractionation between oil–cracking ethane and kerogen is larger than that between kerogen–cracking ethane and kerogen, the carbon isotope of oil–cracking ethane in oil–cracking gas is generally 3‰–5‰ lighter than that of kerogen (Dai et al., 2005). Consequently, the carbon isotope of ethane in P_2l gas should range from –29‰ to –26‰, which is inconsistent with the ethane characteristics of the gas in the MX Gas Field. Moreover, the P_2l gas in the CRSB has not entered the over mature stage, while the dryness coefficients of T_2j^2 and T_2l^1 gases are very high. Therefore, the P_2l source rock is unlikely to be the main source rock in this area. Thus, E_1q is the most important source rock for the Triassic gas reservoirs in the CRSB.

By comparing the characteristics of $\delta^{13}C_1$ and $\delta^{13}C_2$ (Figure 3A, B), the Triassic gases are found to closely resemble the P_2m gases from the WJB and HWC in western Sichuan, and the E_1l gas. Previous research indicates that these gases share a common origin from the E_1q source rock. Specifically, the P_2m gases are oil–cracking gases generated during the early phase of the E_1q 's hydrocarbon generation process, while the E_1l gas represents shale gas released in the late stage of the E_1l maturation (Shuai et al., 2022; Guo et al., 2024). As illustrated in the $\delta^{13}C_{2-1}$ vs. $\delta^{13}C_1$ diagram (Figure 3B), in contrast to oil – cracking gases, the late – stage shale gas in the E_1l Fm exhibits distinct characteristics. It has heavier methane isotopes, reversed carbon isotope ratios between methane and ethane ($\delta^{13}C_1 > \delta^{13}C_2$), and a notably high dryness coefficient (>0.9995), as shown in Figure 3C.

LHs are a crucial component of oil and natural gas, generally referring to C_5 – C_{10} compounds with a boiling point less than 200°C. They contain abundant geochemical information and are often used for origin identification (Hu et al., 2007; Dai et al., 2016), organic matter type determination (Hill et al., 2007), and oil–gas source correlation. Sapropelic parent materials are rich in normal alkanes, while humic parent materials are abundant in isoparaffins, naphthenes, and aromatics (Leythaeuser et al., 1979; Snowdon and Powell, 1982). The triangular diagram of C_{6-7} normal alkanes, isoparaffins, and naphthenes is commonly used to characterize the genetic types of natural gas. In the triangular diagram of C_7 compounds, MCH is derived from the lignin, cellulose, and sugars of higher plants and has stable thermodynamic properties. DMCP comes from the cyclic lipid compounds in sterols and terpenoids of aquatic organisms, and its abundant presence is an important characteristic of oil–type gas. The parent sources of nC_7 are complex, mainly including bacteria, algae, and the chain–like complexes of higher plants. However, it is quite sensitive to maturity and will undergo extensive cracking at high maturity levels (Dai et al., 1992; Odden et al., 1998; Whiticar, 1999; Mango, 2000; Hu et al., 2007). When natural gas reaches the over mature stage, such as the shale gas in the S_1l in southern Sichuan, light hydrocarbons undergo intense thermal cracking. The normal alkanes that originally reflect the sapropelic parent material source are destroyed, and the contents of compounds with strong thermochemical stability, such as naphthenes and aromatics, increase significantly. This distorts

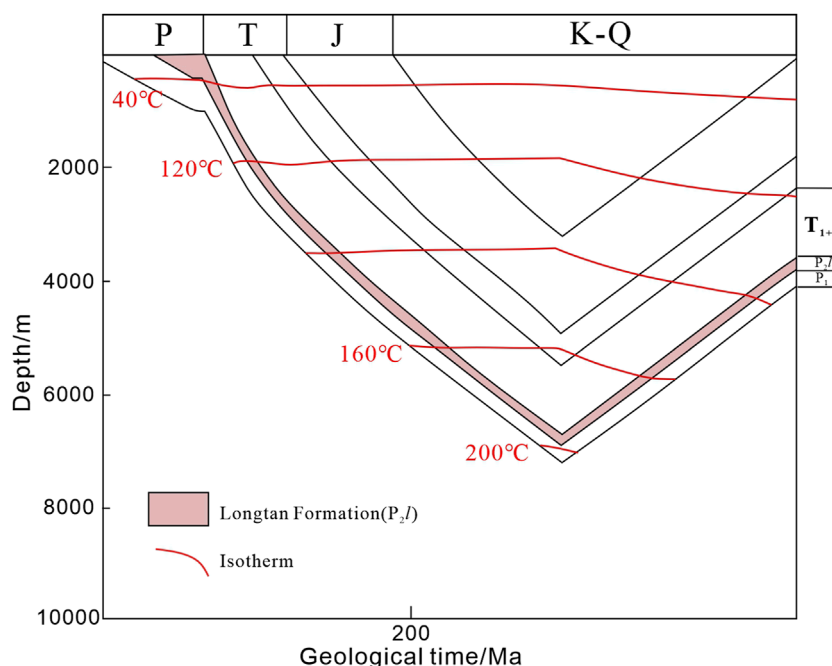


FIGURE 5

Burial and thermal histories, and hydrocarbon charging stages from Well GS17 in CRSB [Burial history and thermal evolution history are modified from Yang et al. (2020)].

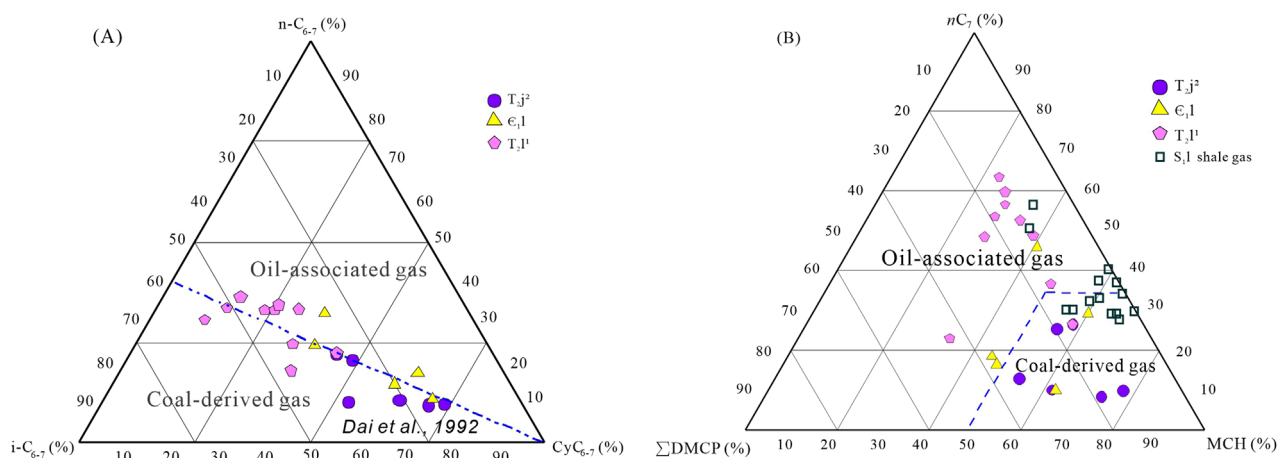


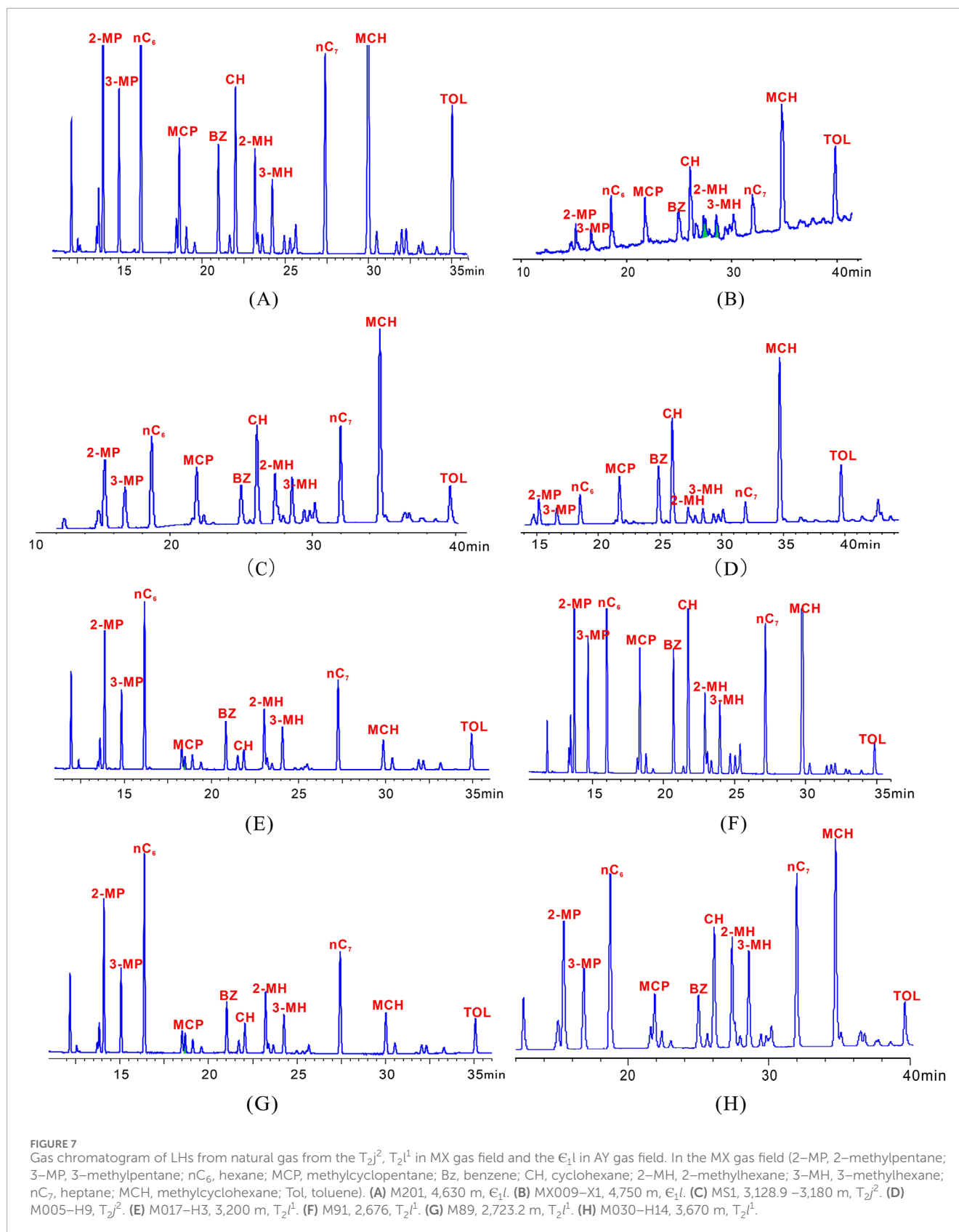
FIGURE 6

Ternary diagram of C_{6-7} (A) and ternary diagram of C_7 (B) LHs associated with natural gas from the T_{2j^2} , T_{2l^1} in MX gas field and the E_{1l} in AY gas field MX gas field [modified after Dai et al. (1992)]. For comparison, we collect the LHs data of typical oil-type gases from Longmaxi shale gas from Dai et al. (2016). ($n-C_{6-7}$, normal C_{6-7} alkanes; $i-C_{6-7}$, branched C_{6-7} alkanes; CyC_{6-7} , C_{6-7} cycloalkanes; $n-C_7$, heptane; DMCPs, dimethylcyclopentanes; MCH, methylcyclohexane).

the identification results of LHs, causing them to fall into the coal-derived gas region (Dai et al., 2016; Figures 6A, B).

In the genetic identification chart of the LHs triangular diagram, the gases of T_{2j^2} and E_{1l} show a high degree of kinship correlation and also have a MCH advantage (Figures 7A–D), falling into the coal-derived gas region. However, the relative contents of normal and isoparaffins in T_{2l^1} gas are relatively high (Figure 7E–H), and the majority of samples fall into the identification region of oil-type gas. Whiticar and Snowdon (1999) proposed that the individual

carbon isotopes of LHs from similar organic sources are highly correlated. In this study, the carbon isotope values of seven LHs compounds, namely, 2–MP, 3–MP, nC_6 , MCP, CH, nC_7 , and MCH, were compared (Table 2; Figure 8B) to observe whether there were differences in gas sources. Ignoring the isotope differences among different LHs compounds, the individual carbon isotope fingerprint diagram of LHs indicates that the T_{2l^1} LHs should be from the same gas source, with their $\delta^{13}C_{MCP} > -24\text{‰}$ and $\delta^{13}C_{MCP} > \delta^{13}C_{CH}$. In contrast, the T_{2j^2} and E_{1l} gases exhibit the characteristics of $\delta^{13}C_{CH}$



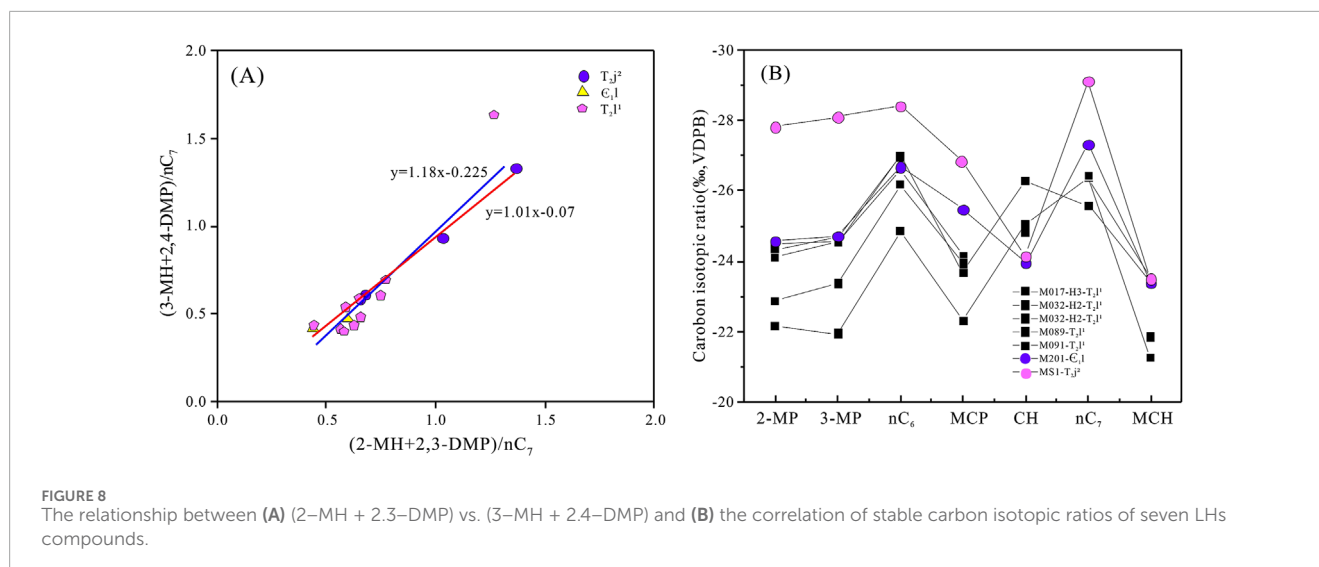


FIGURE 8
The relationship between (A) (2-MH + 2.3-DMP) vs. (3-MH + 2.4-DMP) and (B) the correlation of stable carbon isotopic ratios of seven LHS compounds.

$>-24\%$ and $\delta^{13}C_{MCP} < \delta^{13}C_{CH}$. Based on this, it can be judged that the gas sources of T_2j^2 and T_2l^1 are different, and both T_2j^2 and E_1q gases are derived from the shale gas of E_1q .

The Mango coefficient K_1 , proposed by (Mango, 1997), demonstrates a consistent K value within the same category of oil and gas, yet varies across different types. This characteristic renders it a reliable criterion for gas-source correlation. When examining the diagrams of (2-MH + 2.3-DMP)/ nC_7 versus (3-MH + 2.4-DMP)/ nC_7 (Figures 4A, B), distinct correlations emerge. For the T_2j^2 and E_1l gas samples, the correlation equation is $y = 1.01x - 0.07$, with a high correlation coefficient of $R^2 = 0.9865$, and the average K_1 value of the natural gas is 1.11. In contrast, for the T_2l^1 gas, the correlation relationship is described by $y = 1.18x - 0.225$, with a correlation coefficient of $R^2 = 0.9384$, and the average K_1 value of the natural gas is 1.28. These differences in correlation equations and K_1 values can potentially provide insights into the unique characteristics and origins of each gas sample (Figure 8A).

Based on the above evidence of LHS, it is considered that the sources of T_2j^2 and T_2l^1 natural gases are not completely the same. Although both gases are derived from the E_1q , the gas in T_2l^1 has the admixture of other oil-type gases, and the maturity of this mixed gas is lower than that of the shale gas from the E_1q Fm. However, considering the characteristics of CH_4 and C_2H_6 in natural gas, T_2l^1 gas is significantly different from the gas from the P_2l Fm (LG) and is more similar to the oil-cracking gas and shale gas from the E_1q . It is believed to be formed by the mixing of oil-cracking gas with lower maturity and shale gas. This also well explains the reversal phenomenon observed in the gas from the T_2l^1 .

6 Conclusion

1. The natural gas components in the Triassic gas reservoirs of the MX gas field in central Sichuan are mainly alkane gases. The gas is extremely dry (dryness coefficients ranges from 0.9970 to 0.9985) with a low content of non-alkane gases, mainly being CO_2 and N_2 . All the gas is of oil-type gas and belongs to crude oil-cracking gas.

2. The E_1q Fm is the principal source rock, generating different types of natural gas. It includes both oil-cracking gas (reservoir gas) and shale gas (unaffected by TSR). These two types of gas exhibit diverse geochemical characteristics. The oil-cracking gas is characterized by relatively light $\delta^{13}C_1$ ($<-35\%$), a relatively low dryness coefficient (<0.9995), and a normal sequence of carbon isotopes ($\delta^{13}C_1 < \delta^{13}C_2$). The shale gas has heavy $\delta^{13}C_1$ ($>-35\%$), a high dryness coefficient (>0.9995), and shows carbon isotopes reversal ($\delta^{13}C_1 > \delta^{13}C_2$).
3. The shale gas, with a higher thermal evolution degree, has low abundances of normal and iso-alkanes and a higher proportion of cycloalkanes. Its has the feature of individual carbon isotopes with $\delta^{13}C_{CH} > -24\%$ and $\delta^{13}C_{MCP} < \delta^{13}C_{CH}$, while the oil-cracking gas shows $\delta^{13}C_{MCP} > -24\%$ and $\delta^{13}C_{MCP} > \delta^{13}C_{CH}$.
4. The T_2j^2 gas comes from the shale gas of the E_1q Fm. The T_2l^1 gas is a mixture of oil-cracking gas and shale gas from the E_1q Fm, and this mixture is the main cause of the carbon isotope reversal in the T_2l^1 gas.

Data availability statement

The original contributions presented in the study are included in the article/supplementary material, further inquiries can be directed to the corresponding authors.

Author contributions

CG: Conceptualization, Formal Analysis, Funding acquisition, Investigation, Methodology, Resources, Visualization, Writing-original draft, Writing-review and editing. GH: Data curation, Funding acquisition, Investigation, Methodology, Project administration, Resources, Writing-review and editing. JL: Methodology, Writing-review and editing. XT: Data curation, Investigation, Resources, Supervision, Writing-review and editing. LT: Data curation, Methodology, Software, Supervision, Visualization, Writing-review and editing. JG: Formal Analysis,

Methodology, Writing–review and editing. HC: Data curation, Resources, Writing–review and editing. ZL: Methodology, Writing–review and editing. XL: Funding acquisition, Supervision, Writing–review and editing.

Funding

The author(s) declare that financial support was received for the research and/or publication of this article. The author(s) disclosed receipt of the following financial support for the research, authorship, and/or publication of this article: This work was supported by the National Natural Science Foundation of China (U22B6002), PetroChina Science and Technology Projects (2023ZZ0203, 2021DJ0601, 2021DJ0602) and the Fundamental Research Funds for the Central Universities (Ph.D. Top Innovative Talents Fund of CUMTB NO. BBJ2024044). The authors declare that this study received funding from PetroChina. The funder was not involved in the study design, collection, analysis, interpretation of data, the writing of this article, or the decision to submit it for publication.

Acknowledgments

The authors extend their gratitude to the Research Institute of Exploration and Development.

References

- Bernard, B. B., Brooks, J. M., and Sackett, W. M. (1978). Light hydrocarbons in recent Texas continental shelf and slope sediments. *J. Geophys. Res. Oceans* 83, 4053–4061. doi:10.1029/jc083ic08p04053
- Chen, J., Wang, X., Chen, J., Ni, Y., Xiang, B., Liao, F., et al. (2021). New equation to decipher the relationship between carbon isotopic composition of methane and maturity of gas source rocks. *Sci. China Earth Sci.* 64, 470–493. doi:10.1007/s11430-020-9692-1
- Clayton, C. (1991). Carbon isotope fractionation during natural gas generation from kerogen. *Mar. Petroleum Geol.* 8, 232–240. doi:10.1016/0264-8172(91)90010-x
- Dai, J. (1993). Carbon and oxygen isotopic characteristics and identification of natural gas. *Nat. Gas. Geosci.* 4, 1–40.
- Dai, J., Ni, Y., and Zou, C. (2012). Stable carbon and hydrogen isotopes of natural gases sourced from the Xujiahe Formation in the Sichuan Basin, China. *Org. Geochem.* 43, 103–111. doi:10.1016/j.orggeochem.2011.10.006
- Dai, J., Pei, X., and Qi, H. (1992). Natural Gas Geology of China. Beijing, China: Petroleum Industry Press, 1–280 (in Chinese).
- Dai, J., Qin, S., Tao, S., Zhu, G., and Mi, J. (2005). Developing trends of natural gas industry and the significant progress on natural gas geological theories in China. *Nat. Gas. Geosci.* 16, 127–142.
- Dai, J., Zou, C., Dong, D., Ni, Y., Wu, W., Gong, D., et al. (2016). Geochemical characteristics of marine and terrestrial shale gas in China. *Mar. Petroleum Geol.* 76, 444–463. doi:10.1016/j.marpetgeo.2016.04.027
- Deng, Y., Hu, G., and Zhao, C. (2018). Geochemical characteristics and origin of natural gas in Changxing–Feixianguan formations from Longgang gasfield in the Sichuan Basin, China. *Nat. Gas. Geosci.* 29, 892–907. doi:10.11764/j.issn.1672-1926.2018.03.016
- Fu, X., Chen, Y., Luo, B., Wenzheng, Li., Zhang, J., Wang, X., et al. (2021). Characteristics and petroleum geological significance of the high-quality source rocks in the Gufeng Member of the Middle Permian Maokou Formation in the northern Sichuan basin. *Acta Geol. Sin.* 95, 1903–1920. doi:10.19762/j.cnki.dizhixuebao.2021128
- Guo, C., Hu, G., Tian, X., Tian, L., Guo, J., and Li, X. (2024). The geochemical differences and origin of multilayered natural gases in marine strata, the northwestern Sichuan Basin, China. *Energy Explor. and Exploitation* 42, 401–428. doi:10.1177/01445987231185798
- Hill, R. J., Jarvie, D. M., Zumberge, J., Henry, M., and Pollastro, R. M. (2007). Oil and gas geochemistry and petroleum systems of the Fort Worth Basin. *AAPG Bull.* 91, 445–473. doi:10.1306/11030606014
- Hu, G., Li, J., Li, J., Li, Z., and Luo, X. (2007). Discussion on the light hydrocarbons index in the identification of natural gas. *Sci. China D.* 37, 111–117. doi:10.1360/zd2007-37-zkII-111
- Hu, G., Li, J., Shan, X., and Han, Z. (2010). The origin of natural gas and the hydrocarbon charging history of the Yulin gas field in the Ordos Basin, China. *Int. J. Coal Geol.* 81, 381–391. doi:10.1016/j.coal.2009.07.016
- Hu, G., Xiao, Z., Luo, X., Li, Z., Li, J., Sun, Q., et al. (2005). Light hydrocarbon composition difference between two kinds of cracked gases and its application. *Nat. Gas. Ind.* 25, 23–25.
- Hu, G., Yu, C., Ni, Y., Huang, S., and Tian, X. (2013). Comparative study of stable carbon and hydrogen isotopes of alkane gases sourced from the Longtan and Xujiahe coal-bearing measures in the Sichuan Basin, China. *Int. J. Coal Geol.* 116–117, 293–301. doi:10.1016/j.coal.2013.07.006
- Huang, S., Zhao, Z., Ai, Y., Jiang, H., Tian, X., Jiang, Q., et al. (2024). Differences in gas sources of the changxing–feixianguan formations around the Kajiang–Liangping trough and favorable exploration directions for coal–formed gas generated by the upper Permian Longtan Formation, Sichuan Basin, China. *J. Nat. Gas Geoscience* 9, 321–331. doi:10.1016/j.jnggs.2024.09.001
- Jiao, F., Yang, Y., Ran, Q., Wu, G., and Liang, H. (2022). Distribution and gas exploration of the strike–slip faults in the central Sichuan Basin. *Nat. Gas. Ind.* 9, 63–72. doi:10.1016/j.ngib.2021.08.018
- Jin, H., Dai, H., and Wen, H. (2019). Summary of reservoir–forming characteristics of Moxi Leikoupo formation gas reservoir in central Sichuan. *Chem. Eng. Des. Commun.* 45, 240–241.
- Leythaeuser, D., Schaefer, R. G., Cornford, C. t., and Weiner, B. (1979). Generation and migration of light hydrocarbons (C₂–C₇) in sedimentary basins. *Org. Geochem.* 1, 191–204. doi:10.1016/0146-6380(79)90022-6

Conflict of interest

Authors CG, GH, JL, LT, JG, HC, and ZL were employed by PetroChina Research Institute of Petroleum Exploration and Development. Author XT was employed by PetroChina Southwest Oil & Gas field Company.

The remaining author declares that the research was conducted in the absence of any commercial or financial relationships that could be construed as a potential conflict of interest.

Generative AI statement

The author(s) declare that no Generative AI was used in the creation of this manuscript.

Publisher's note

All claims expressed in this article are solely those of the authors and do not necessarily represent those of their affiliated organizations, or those of the publisher, the editors and the reviewers. Any product that may be evaluated in this article, or claim that may be made by its manufacturer, is not guaranteed or endorsed by the publisher.

- Li, Q., Li, B., Mei, W., and Liu, Y. (2022). Genesis and sources of natural gas in fold-and-thrust belt: the Middle Permian in the NW Sichuan Basin. *Mar. Petroleum Geol.* 140, 105638. doi:10.1016/j.marpetgeo.2022.105638
- Li, Y., Liang, Y., Lei, B., Guo, G., and Luo, Y. (2006). Natural gas genesis for the section II of west jialingjiang formation in middle sichuan-south sichuan transitional belt. *J. Nat. Gas Geoscience* 17, 820–823.
- Liu, Q., Worden, R. H., Jin, Z., Liu, W., Li, J., Gao, B., et al. (2014). Thermochemical sulphate reduction (TSR) versus maturation and their effects on hydrogen stable isotopes of very dry alkane gases. *Geochimica Cosmochimica Acta* 137, 208–220. doi:10.1016/j.gca.2014.03.013
- Liu, Q., Zhijun, J., Jianfa, C., Krooss, B. M., and Qin, S. (2012). Origin of nitrogen molecules in natural gas and implications for the high risk of N₂ exploration in Tarim Basin, NW China. *J. Petroleum Sci. Eng.* 81, 112–121. doi:10.1016/j.petrol.2011.12.013
- Lu, X., Gui, L., Wang, Z., Liu, S., Liu, Q., Fan, J., et al. (2024). Activity time of strike-slip faults and their controlling effects on hydrocarbon accumulation in central Sichuan Basin: evidence from U–Pb dating and fluid inclusions of cements in fault zone. *Acta Pet. Sin.* 45, 642. doi:10.7623/syxb202404003
- Ma, D., Wang, Z., Duan, S., Gao, J., Jiang, Q., Jiang, H., et al. (2018). Strike-slip faults and their significance for hydrocarbon accumulation in Gaoshiti–Moxi area, Sichuan Basin, SW China. *Petroleum Explor. Dev.* 45, 851–861. doi:10.1016/s1876-3804(18)30088-0
- Mango, F. D. (1997). The light hydrocarbons in petroleum: a critical review. *Org. Geochem.* 26, 417–440. doi:10.1016/s0146-6380(97)00031-4
- Mango, F. D. (2000). The origin of light hydrocarbons. *Geochimica Cosmochimica Acta* 64, 1265–1277. doi:10.1016/s0016-7037(99)00389-0
- Milkov, A. V. (2021). New approaches to distinguish shale-sourced and coal-sourced gases in petroleum systems. *Org. Geochem.* 158, 104271. doi:10.1016/j.orggeochem.2021.104271
- Milkov, A. V., Faiz, M., and Etiope, G. (2020). Geochemistry of shale gases from around the world: composition, origins, isotope reversals and rollovers, and implications for the exploration of shale plays. *Org. Geochem.* 143, 103997. doi:10.1016/j.orggeochem.2020.103997
- Ni, Y., Liao, F., Gao, J., Chen, J., Yao, L., and Zhang, D. (2019). Hydrogen isotopes of hydrocarbon gases from different organic facies of the Zhongba gas field, Sichuan Basin, China. *J. Petroleum Sci. Eng.* 179, 776–786. doi:10.1016/j.petrol.2019.04.102
- Odden, W., Patience, R., and Van Graas, G. (1998). Application of light hydrocarbons (C₄–C₁₃) to oil/source rock correlations: a study of the light hydrocarbon compositions of source rocks and test fluids from offshore Mid-Norway. *Org. Geochem.* 28, 823–847. doi:10.1016/s0146-6380(98)00039-4
- Schoell, M. (1980). The hydrogen and carbon isotopic composition of methane from natural gases of various origins. *Geochimica cosmochimica ACTA* 44, 649–661. doi:10.1016/0016-7037(80)90155-6
- Shuai, Y., Li, J., Tian, X., Chen, Z., Zhang, B., and Wei, C. (2022). Accumulation mechanisms of Sinian to Triassic gas reservoirs in the central and western Sichuan basin and their significance for oil and gas prospecting. *Acta Geol. Sin.* 97, 1526–1543. doi:10.19762/j.cnki.dizhixuebao.2023227
- Snowdon, L. R., and Powell, T. G. (1982). Immature oil and condensate—modification of hydrocarbon generation model for terrestrial organic matter. *AAPG Bull.* 66, 775–788. doi:10.1306/03b5a313-16d1-11d7-8645000102c1865d
- Stahl, W. J., and Carey, B. D. (1975). Source-rock identification by isotope analyses of natural gases from fields in the Val Verde and Delaware basins, west Texas. *Chem. Geol.* 16, 257–267. doi:10.1016/0009-2541(75)90065-0
- Thompson, K. F. (1983). Classification and thermal history of petroleum based on light hydrocarbons. *Geochimica Cosmochimica Acta* 47, 303–316. doi:10.1016/0016-7037(83)90143-6
- Wang, S., Dai, H., Wang, T., and Lin, F. (1998). Gas source and migration of high-mature natural gas in Moxi Gas Field. *Pet. Explor.* 3, 5–8.
- Wang, X., Liu, W., Shi, B., Zhang, Z., Xu, Y., and Zheng, J. (2015). Hydrogen isotope characteristics of thermogenic methane in Chinese sedimentary basins. *Org. Geochem.* 83 (84), 178–189. doi:10.1016/j.orggeochem.2015.03.010
- Wang, Z., Xin, Y., Xie, W., Wen, L., Zhang, H., Xie, Z., et al. (2023). Petroleum geology of marl in triassic Leikoupo Formation and discovery significance of well Chongtan1 in central Sichuan Basin, SW China. *Petroleum Explor. Dev.* 50, 1092–1104. doi:10.1016/s1876-3804(23)60451-3
- Wei, G., Xie, Z., Song, J., Yang, W., Wang, Z., Li, J., et al. (2015). Features and origin of natural gas in the Sinian–Cambrian of central Sichuan paleo-uplift, Sichuan Basin, SW China. *Petroleum Explor. Dev.* 42, 768–777. doi:10.1016/s1876-3804(15)30073-2
- Whiticar, M. J. (1999). Carbon and hydrogen isotope systematics of bacterial formation and oxidation of methane. *Chem. Geol.* 161, 291–314. doi:10.1016/s0009-2541(99)00092-3
- Whiticar, M. J., and Snowdon, L. R. (1999). Geochemical characterization of selected western Canada oils by C₂±C₈ compound specific isotope correlation. *Org. Geochem.* 30, 1127–1161. doi:10.1016/s0146-6380(99)00093-5
- Xie, Z., Li, J., Yang, C., Tian, X., Zhang, L., Li, J., et al. (2021). Geochemical characteristics of Sinian–Cambrian natural gas in central Sichuan paleo-uplift and exploration potential of Taihe gas area. *Nat. Gas. Ind.* 41, 1–14. doi:10.37877/j.issn.1000-0976.2021.07.001
- Xie, Z., Yang, C., and Dong, C. (2020). Geochemical characteristics and genesis of middle devonian and middle permian natural gas in Sichuan Basin. *China* 31, 447–461. doi:10.11764/j.issn.1672-1926.2020.01.005
- Xu, A., Hu, S., Wang, Z., Bo, D., Li, M., Lu, W., et al. (2016). Sedimentary mode and reservoir distribution of the Cambrian carbonate and evaporate paragenesis system in the Sichuan Basin. *Nat. Gas. Ind. B* 3, 418–427. doi:10.37877/j.issn.1000-0976.2016.06.002
- Yang, C., Wen, L., Wang, T., Luo, B., Li, M., Tian, X., et al. (2020). Timing of hydrocarbon accumulation for paleo-oil reservoirs in Anyue gas field in Chuazhong Uplift. *Oil and Gas Geol.* 41, 492–502. doi:10.11743/ogg20200306
- Yu, X. (2022). Accumulation mechanism and model of natural gas in the Leikoupo Formation, western depression, Sichuan Basin. PhD thesis. China University of Geosciences: Wuhan, China. doi:10.27492/d.cnki.gzdz.2022.000014
- Zhang, T., Huang, S., Li, X., Jiang, H., Zeng, F., and Ma, Y. (2024). Sedimentary geochemical characteristics and organic matter enrichment of the lower cambrian Qiongzhusi Formation in the Sichuan Basin. *Nat. Gas. Geosci.* 35, 688–703. doi:10.11764/j.issn.1672-1926.2023.09.016
- Zhang, X., Pang, H., Pang, X., Chen, J., Wu, S., Ma, K., et al. (2022). Hydrocarbon generation and expulsion characteristics and resource potential of source rocks in the Longtan Formation of Upper Permian, Sichuan Basin. *Oil and Gas Geol.* 43, 621–632. doi:10.11743/ogg20220311